Collisional ionization and destruction cross sections for hydrogen and helium Rydberg atoms on Ar, Xe, and N_2: Failure of the independent-particle model

S. P. Renwick,* F. Deng,† H. Martinez,‡ and T. J. Morgan
Department of Physics, Wesleyan University, Middletown, Connecticut 06459
(Received 21 September 1992)

Absolute cross sections for the collisional ionization and the total destruction of hydrogen and helium atoms in low-lying Rydberg states colliding with Ar, Xe, and N_2 have been measured over the energy range from 1.0 to 30 keV/amu. The independent-particle model fails to explain the behavior of the Rydberg atom's outer electron in ionization collisions below 3 keV/amu for He ($12 \leq n \leq 15$) on Xe and N_2, but not on Ar. This represents an observation of the model's failure in collisions of Rydberg atoms with neutral perturbers in this energy range and shows that at low energies, where a molecular picture of the core-target scattering is valid, the Rydberg electron is sensitive to details of the molecular interactions between the target and the Rydberg atom's core.

PACS number(s): 34.50.−s, 34.80.−i, 34.60.+z, 34.70.+e

I. INTRODUCTION

The application of independent-particle models to the analysis of complicated physical phenomena is widespread, with resulting interest in the areas over which such models can be expected to be valid. The Rydberg atom, with its widely separated core and Rydberg electron, has in the past provided a fertile ground for the use of such models [1]. Specifically, such a model, referred to here as *the* independent-particle model (IPM) has in the past [2–5] been applied to fast collisions of Rydberg H and He atoms and molecules with neutral targets; the independent particles are, of course, the projectile Rydberg atom's core and outer electron. Hitherto, the IPM has been successful in describing *fast* collisions between *neutral* Rydberg atoms. A similar "free-electron" model, wherein the Rydberg electron behaves as a quasifree electron carried into a collision by a spectator core, has been successfully used for thermal energy collisions [1], although recently Pesnelle *et al.* have found regimes where that model breaks down [6]. Collisions between fast ions and neutral Rydberg atoms have been studied by MacAdam, Gray, and Rolfes [7], but do not appear amenable to simple IPM analysis due to the longer-ranged Coulomb interaction. We present results of further experiments as an extension of the applicability of IPM to fast neutral collisions; we now have found regimes where it is no longer valid.

The model itself, described by Matsuzawa [8], is appealingly simple. The Rydberg atom is viewed as two separate quasifree particles—a singly charged ionic core (here H^+ or He^+) and a companion electron. No connection between the two is made other than that they are traveling at the same speed in a beam. The collision can then consist of either of two separate events: a collision of either the ion or the electron with the neutral target. Under IPM, neither event is affected by the presence of the companion particle. Subtle effects may, however, be present: the present work shows that although the colliding partners are unaffected by the spectator, the spectator may be affected by the details of the collision.

It is easy to see why this model is reasonable. The radius of the Rydberg electron's orbit can be estimated from the Bohr model as $n^2 a_0$, where n is the atom's principal quantum number and a_0 is the Bohr radius. For atoms with n ranging from 10 to 20, this leads to orbital radii on the order of 100 Å. Since, however, the effective range of interaction of the projectile's component charged particles with the neutral target is on the order of several Å, one immediately sees that the Rydberg atom is simply too big to interact with a neutral target as a single object. The use of beams of Rydberg atoms with energies of a few keV frequently affords a further simplification in that, under certain conditions, the Rydberg atom is effectively "frozen" during the collision. For H and He in the present study, the magnitude V of the velocity $\mathbf{V}$ of the projectile atoms ranges from 0.2 a.u. at 1 keV/amu to 1.1 a.u. at 30 keV/amu, the energy range used. The laboratory-frame velocity $\mathbf{v}$ of the Rydberg electron will be given by $\mathbf{V}$ modified by the electron's effective orbital velocity $\mathbf{v}_e$ calculated from its momentum distribution in the particular Rydberg state: $\mathbf{v}=\mathbf{V}+\mathbf{v}_e$. The magnitude v_e of the velocity $\mathbf{v}_e$, though, can be estimated from the Bohr model as $1/n$ atomic units ($12 \leq n \leq 15$ in this experiment). We see that, then, for much of the range given, $v_e \ll V$, and hence $v \approx V$: for example, the electron in a Rydberg atom with $n=15$ in a 15-keV/amu beam would have $v_e/V \approx 0.09$. Thus, in an electron-target collision (according to IPM), the target not only sees the electron alone, unaffected by the core, but also sees it traveling at the beam velocity (yielding, for example, electron kinetic energies of 0.6–12 eV in this experiment). In the present study, the lowest beam energy was 1.0 keV/amu and the lowest principal quantum number n equal to 12, making the largest $v_e/V \approx 0.42$; this took the low-energy results of the experiment out of the range of validity of the frozen-atom model.

Consider the example of the measurement of two cross sections from a H Rydberg atom's collision: the total de-

struction cross section σ_d and the collisional ionization cross section σ_i. Ionization will proceed through quasi-free scattering of the Rydberg electron, as virtually any scattering mechanism will cause the weakly bound electron to leave the atom:

$$H^* + X \rightarrow H^+ + X + e \ .$$

The Rydberg atom's ionization cross section is then given by the equal-velocity free-electron total scattering cross section; with m the electron mass, M the Rydberg atom mass, and E the beam energy, we have

$$\sigma_i(E) = \sigma_e \left[\frac{m}{M} E \right] . \quad (1)$$

Core scattering can also destroy the Rydberg atom. The primary collision mechanism for protons in the keV range is electron capture, with cross section σ_{10}. If electron capture by the Rydberg atom core occurs, the Rydberg electron will suddenly find its Coulomb field missing, and will wander off:

$$H^* + X \rightarrow H + X^+ + e \ .$$

The two scattering processes combine incoherently to yield the destruction cross section

$$\sigma_d(E) = \sigma_{10}(E) + \sigma_e \left[\frac{m}{M} E \right] . \quad (2)$$

Note that, with typical few-keV kinetic-energy electron-capture cross sections on the order of a few Å^2, and with few-eV kinetic-energy free-electron-scattering cross sections ranging from about 0.1 to 50 Å^2, σ_d will always be less than 50 to 60 Å^2. This is substantially less than the Rydberg atom's geometrical cross section of order 10 000 Å^2.

Previous experiments at high quantum numbers by Koch [2] showed that ionization cross sections for 3.75–5.5 keV/amu D ($35 \leq n \leq 50$) atoms colliding with N_2 followed experimental cross sections for equal-velocity free electrons scattering from N_2 quite well, verifying Eq. (1). Measurements of destruction cross sections for D ($n = 46$) atoms on N_2 showed good agreement with Eq. (2). Later measurements of σ_d for intermediate quantum numbers were conducted in this laboratory for H ($19 \leq n \leq 35$) colliding with Ar, N_2, CO_2, and SF_6 [3] as well as He^* and H_2^* on Ar, N_2, and SF_6 [4]. Finally, Silim and Latimer [5] have recently measured σ_d for He ($10 < n < 20$) atoms colliding with N_2, He, Ar, and Xe. All of the destruction cross-section experiments have verified Eq. (2) in cases where electron-capture cross sections were available. In the case where σ_{10} was not available, the SF_6 target, σ_d followed the general shape of the electron-scattering cross section with an offset, as would be expected. Recent electron-capture data [9] are consistent with IPM predictions for this target as well. Note that the different targets all exhibit qualitatively and quantitatively different behavior in their electron scattering, suggesting that the validity of IPM does not depend on the precise type of electron-scattering mechanism for interactions with neutral targets. For the Xe and Ar targets especially, though, the destruction mechanism is dominated at low collision energies by the core collision channel. We wish therefore to measure the electron-scattering ionization channel independently as a more stringent test of IPM.

We have improved our apparatus by extending the range of the detectable Rydberg atom band to lower n and by making absolute measurement of the ionization cross section σ_i feasible. We have conducted measurements of both σ_d and σ_i for low-lying Rydberg states of H and He [H ($13 \leq n \leq 16$) and He ($12 \leq n \leq 15$)] colliding with Ar, Xe, and N_2, and have now observed significant deviations from the independent-particle model's predictions in the cases of He on Xe and N_2.

II. APPARATUS

Hydrogen or helium ions are produced in a duoplasmatron ion source, extracted, and accelerated to the desired energy between 4 and 40 keV. After momentum analysis in the field of a dipole bending magnet the ions are sent into the experimental apparatus shown schematically in Fig. 1. Neutral atoms are produced by charge exchange in a sodium-vapor cell of length 4.6 cm, typically maintained at a vapor pressure of about 1 mTorr. The electron capture, as is well known, produces not only ground-state atoms but also excited states with a n^{-3} distribution [10–12]; thus, a small fraction (<1%) of the neutral atoms are in the desired Rydberg states. Remain-

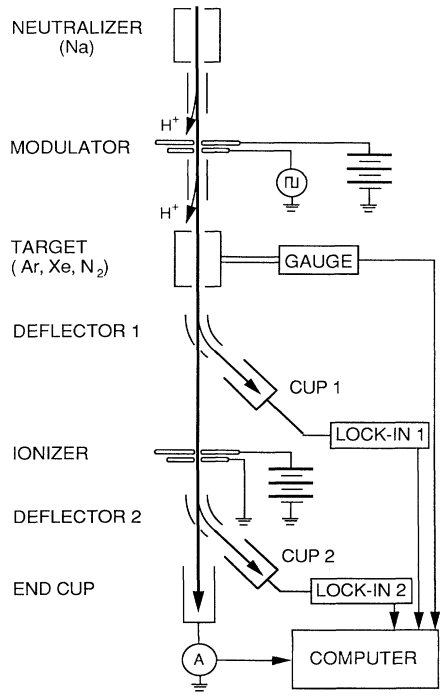

FIG. 1. Experimental apparatus. Momentum-analyzed H^+ or He^+ ions of energy 4–40 keV enter the apparatus from the top. LOCK-IN denotes a lock-in amplifier and A an ammeter.

ing ions are swept out of the beam by a pair of electric-field plates after the cell.

We then need to distinguish atoms in the desired band of Rydberg states from the rest of the beam. This is accomplished in the *modulator* through the use of field ionization. In this region is an axial electric field F produced by two parallel plates which are perpendicular to the beam axis, separated by 2.2 mm, and which have central 1.5-mm holes through which the beam passes. This field F will ionize all Rydberg atoms in states with principal quantum number n greater than or equal to a critical $n_c(F)$. Superimposed on a large constant electric-field component is a square wave, which modulates the field between two values, $F_{\rm hi}$ and $F_{\rm lo}$. This produces a modulated band of Rydberg atoms with quantum numbers between $n_c(F_{\rm hi})$ and $n_c(F_{\rm lo})$ within the available distribution. Ions produced in this region are swept out of the beam by a second set of plates.

Collisions took place in a second cell, of length $l=5$ cm, into which the target gas was admitted through a fine-control valve. Target gas pressure was measured absolutely by a Baratron capacitance manometer; data were taken with the pressure between 0 and 3 mTorr. The gas-handling system allowed quick switching from one target to another with the beam running, which facilitated *in-situ* target comparisons.

Neutral Rydberg atoms leaving the target are then ionized in the *ionizer* (see Fig. 1), physically almost identical to the modulator, where a static electric field high enough to ionize all atoms in the modulated band was maintained. Those ions are then sent by the second deflector shown in Fig. 1 into a Faraday cup, denoted "cup 2," from whose output a lock-in amplifier extracts the modulated Rydberg atom signal. The current from the neutral atoms in the beam is measured by an end cup biased to detect neutral atoms via secondary-electron emission.

In both the modulator and the ionizer, since the beam passed through apertures in the plates, the field F experienced by the beam atoms is less than the parallel-plate field $F_{\rm PP}$ far from the holes in the plates' centers. It was necessary to know the coefficient $F/F_{\rm PP}$. This coefficient was determined using two methods, the first being the use of physical measurements of plots of equipotential lines from two sources: a commercial field-line calculating program and an equipotential-plotting apparatus designed for instructional use. Agreement between the two sets of equipotential lines was excellent. The second method used the Rydberg atoms themselves. The field in the first deflector (see Fig. 1), because of the deflector's simple geometry, is easily known accurately. The modulated atomic band was set to a fixed width and a modulated signal from Rydberg atoms measured in cup 2; the field in deflector 1 was then increased to the point where it nulled the signal by ionizing and removing all the Rydberg atoms before they could be detected. At that point the modulator and deflector fields were equal and the coefficient could be determined. A similar procedure was used for the ionizer. These two methods agreed quite well, yielding $F/F_{\rm PP}=0.85\pm0.03$ in both the modulator and ionizer. All field values cited herein are those experienced by the beam atoms.

As a further calibration, a field-ionization spectrum can be made by setting the square wave's amplitude as small as practicable and scanning the resulting narrow modulation through the available field range. Such a spectrum for H* is shown in Fig. 2, in which the modulation amplitude ranged from 0.25 to 1.0 kV/cm. (The resulting small signal required that cup 2 be replaced with a Channeltron electron multiplier.) The locations of peaks in the spectrum, corresponding to states of differing principal quantum number, agree well with calculations [13] of field ionization for H*. The field required to ionize $H(n)$ can be estimated by the formula

$$F(n)=\frac{1}{8n^4}\ \text{a.u.}\ , \tag{3}$$

which is frequently used [14] to estimate the apparent threshold field exhibited by the H* atom's tunneling ionization process. Similar spectra were produced for He*, where the ionizing field can be estimated by [15]

$$F(n)=\frac{1}{16n^4}\ \text{a.u.} \tag{4}$$

For the collision experiments the modulated band was much wider; typically, $F_{\rm hi}$ and $F_{\rm lo}$ were equal to 25 and 10 kV/cm, respectively, producing a modulated population of H ($13\le n\le 16$) or He ($12\le n\le 15$). This widening of the modulated band was necessary in order to increase the modulated-ion signal to the point where it could be measured with Faraday cups. (An overwhelm-

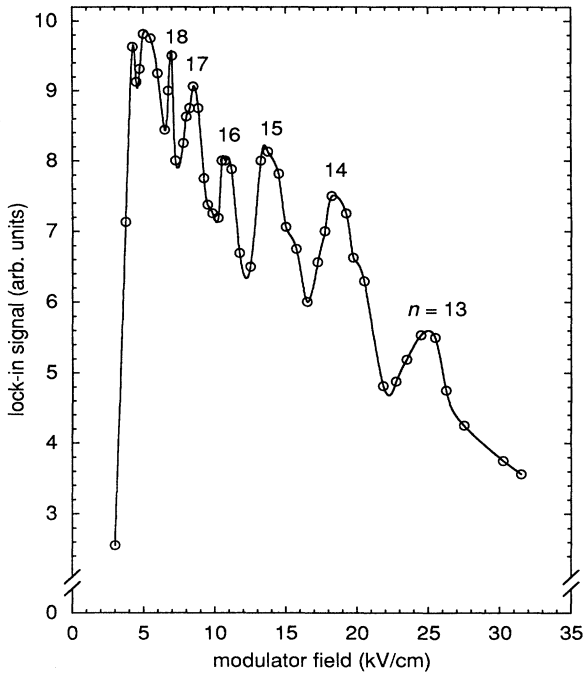

FIG. 2. Field-ionization spectrum of collisionally produced H Rydberg atoms. The line is drawn to guide the eye and has no other significance. Principal quantum numbers are assigned using Eq. (3) in the text. The modulation field amplitude ranged from 0.25 to 1.0 kV/cm.

ing dc background prevented the use of a Channeltron or other electron multiplier in the place of cup 1.)

Measurement of an absolute cross section for Rydberg atom destruction is then simple in principle, since it requires only measurement of the transmitted Rydberg atoms versus target pressure. Rydberg atoms surviving passage through the gas cell of length l were ionized in the field ionizer. The resulting ions were deflected into cup 2, and the Rydberg atoms' signal I_r, the modulated part of the Faraday cup current, measured as a function of target pressure P, including $P=0$. The destruction cross section σ_d was then found by fitting data to the transmission equation

$$\ln\left[\frac{I_r(\pi)}{I_r(\pi=0)}\right]=-\sigma_d\pi\ , \tag{5}$$

where the target thickness $\pi=Pl$. The neutral beam current (mainly ground-state atoms) was monitored with the end cup, and Rydberg atom currents were normalized to it to account for beam drift. Secondary collision effects would involve repopulation of the Rydberg band by electron capture or collisional excitation. The cross sections for both these processes are quite small: cross sections for electron capture to Rydberg states [10] and those for collisional excitation [16] are both on the order of 10^{-3} Å^2. Thus, maintaining the target cell at low enough pressure to exclude secondary collisions was not difficult; the signal showed no consistent deviation from Eq. (5) even at the highest cell pressures used. A sample of destruction data fitted to Eq. (5) is shown in Fig. 3.

Measurement of an absolute ionization cross section is not as simple; it was performed as follows. Ions leaving the target were deflected out of the beam ahead of the ionizer (see Fig. 1) and sent into another Faraday cup ("cup 1"), where the modulated ion signal I_+—ions produced from modulated Rydberg atoms—was measured and normalized to $I_r(\pi=0)$. Care had to be taken to ensure that I_+ and $I_r(0)$ were measured with the same efficiency; although the cups had the same efficiency, namely, 1, two additional effects had to be considered.

The first effect involves the electric fields in use. A band of atomic states is selected in the modulator, after which the selected atoms enter a region of zero electric field, allowing the Stark substates in the band to become degenerate. It was found that the atoms would shift substates in passage from the modulator to the ionizer, moving into states ionized by fields higher or lower than the limits of the modulating field. That is, the modulated band of states widens. The high-n limit of the detected Rydberg atom band is set by the small field in the first deflector, and the low-n limit by the large field in the field ionizer. It was empirically found that maintaining the ionizer field about four times higher than the high modulation field (i.e., usually at 100 kV/cm) and maintaining the low modulation field four times higher than the deflector field was enough to saturate the Rydberg atom signal, thus ensuring that the modulated ions detected in cup 1 corresponded to the band of modulated Rydberg atoms detected at zero target pressure in cup 2. That is, the detection field limits were widened in order to accommodate the spread-out Rydberg atom band. These field ratios are consistent with calculations from known field-ionization behavior for Rydberg hydrogen [13] and hydrogenic atoms [15].

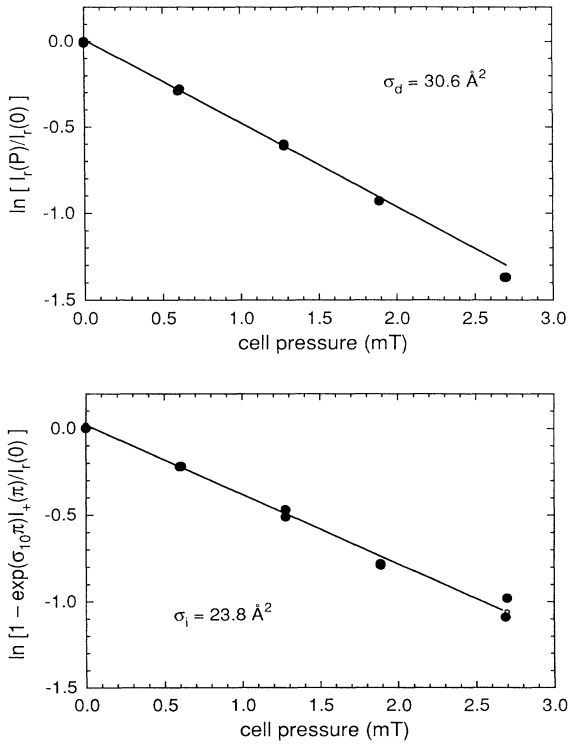

FIG. 3. Sample experimental data: 6 keV/amu He* on Xe. The upper graph shows data used to measure the destruction cross section via Eq. (5), while the lower graph shows data used to measure the ionization cross section via Eq. (14). Cross sections are directly proportional to the slope of the straight line on each graph. The data were collected simultaneously.

Another effect comes from the geometry of the ionizer, which was originally designed for application of much higher fields ($\sim$250 kV/cm) than in the present study. Limits on the high voltage applied to the plates required that the plates be close together (2.2-mm separation), which in turn required that the holes through the plates allowing passage of the beam could not be too large (1.5-mm diameter). Bigger holes would reduce the size of the electric field on axis; recall that already the on-axis field was smaller than the parallel-plate field by a factor of 0.85. This all meant that the holes did not allow all of the Rydberg atom beam to pass the ionizer; $I_r(0)$ is reduced by a efficiency $\epsilon=I(\text{cup 2})/I(\text{cup 1})$.

This efficiency was measured for two species: ions and neutral Rydberg atoms. In the first measurement, a beam of ions was deflected first into cup 1 and second into cup 2 and the ratio of the observed currents taken to find the ion efficiency ϵ_i. It is possible to measure Rydberg atoms without the ionizer by ionizing them in the deflector fields; this method was used to send ionized Rydberg atoms into the two cups and derive a Rydberg efficiency ϵ_r. We found that $\epsilon_i=0.71\pm0.15$ and $\epsilon_r=0.66\pm0.05$.

The Rydberg efficiency showed no energy-dependent trend, while the ion efficiency showed a slight downward trend as beam energy went down. A value of $\epsilon=0.67$ was used for all cross-section measurements; the output current of cup 2 was divided by ϵ.

After taking efficiencies into account, undesired effects on the signal were considered, the first being that of secondary collisions. In the absence of secondary collisions, the ionization cross section σ_i could be extracted by fitting the measured modulated-ion current $I_+(\pi)$ to the equation

$$I_+(\pi)=I_r(0)(1-e^{-\sigma_i\pi}) , \tag{6}$$

itself inexact but a good approximation if $(\sigma_{10}\pi)^2\ll 1$, $(\sigma_i\pi)^2\ll 1$, and $\sigma_{10}\sigma_i\pi^2\ll 1$. In contrast to the destruction measurement, though, secondary effects here could not be neglected; keeping the target pressure low enough to ensure single-collision conditions yielded a measurement with an unacceptably large error due to poor signal-to-noise ratio. Two secondary collision mechanisms affect the measurement. Rydberg atoms destroyed in the primary collision through the ionization channel yield modulated ions, which can then capture an electron in a secondary collision. This will decrease the modulated-ion signal. Rydberg atoms destroyed by neutralization yield modulated neutral atoms, primarily in the ground state, which can ionize in a secondary collision and add to the modulated-ion signal.

We must therefore be more careful in extracting σ_i. The differential rate equation governing production and loss of modulated ions is

$$dI_+=\sigma_i I_r(\pi)d\pi-\sigma_{10}I_+(\pi)d\pi+\sigma_{01}I_g(\pi)d\pi , \tag{7}$$

where σ_{01} is the cross section for collisional ionization of ground-state atoms, σ_{10} is the electron-capture cross section, and $I_g(\pi)$ represents the current of *modulated* neutral ground-state atoms *produced from Rydberg atoms.* Here we have assumed that destruction of a Rydberg atom results in either an ion or a ground-state neutral. Atoms produced in low-lying non-Rydberg states are counted with the ground-state atoms. This is similar to IPM in that we assume that the two processes' cross sections can be added incoherently; application of IPM would identify σ_i with free-electron scattering [as shown in Eq. (1)] and would identify the neutralization cross section with σ_{10}.

The first term of Eq. (7) represents the primary collisional production of modulated ions, while the other two are the secondary collision mechanisms mentioned above. This is rewritten as

$$\frac{dI_+}{d\pi}+\sigma_{10}I_+(\pi)=\sigma_i I_r(\pi)+\sigma_{01}I_g(\pi) , \tag{8}$$

which we want to solve for I_+. We know $I_r(\pi)$ from Eq. (5) and approximate $I_g(\pi)$ similarly to Eq. (6):

$$I_r(\pi)=I_r(0)e^{-\sigma_d\pi},\quad I_g(\pi)=I_r(0)(1-e^{-\sigma_g\pi}) , \tag{9}$$

where σ_g is the cross section for neutralizing Rydberg atoms. The general solution to Eq. (8) then becomes

$$\begin{aligned}I_+(\pi)=&e^{-\sigma_{10}\pi}\int\sigma_i I_r(0)e^{-\sigma_d\pi}e^{\sigma_{10}\pi}d\pi\\&+e^{-\sigma_{10}\pi}\int\sigma_{01}I_r(0)(1-e^{-\sigma_g\pi})e^{\sigma_{10}\pi}d\pi\\&+Ce^{-\sigma_{10}\pi} .\end{aligned} \tag{10}$$

We now need to identify σ_g. As stated above, we first recognize that the destruction cross section is the incoherent sum of cross sections for the two possible destruction channels: $\sigma_g+\sigma_i=\sigma_d$. Under IPM, $\sigma_g=\sigma_{10}$ exactly. Now, destruction measurements, the accuracy of which does not depend on this secondary-correction analysis, show that IPM is *approximately* obeyed in all cases studied. This is shown by our data in the next section and by the data of Silim and Latimer [5]. We therefore assume that $\sigma_g\approx\sigma_{10}$. Since σ_{10} appears only in a secondary correction and since in the experiments the target was always kept thin enough such that $\sigma_{10}\pi<1$, we believe that this approximate equality will still allow accurate determination of σ_i, and thus set $\sigma_g=\sigma_{10}$. This simplifies the first integral. Evaluating the integrals and using the initial condition that there are no modulated ions at $\pi=0$ gives a solution:

$$\begin{aligned}I_+(\pi)=I_r(0)e^{-\sigma_{10}\pi}\Bigg[&1+\frac{\sigma_{01}}{\sigma_{10}}(e^{\sigma_{10}\pi}-1)\\&-\sigma_{01}\pi-e^{-\sigma_i\pi}\Bigg] .\end{aligned} \tag{11}$$

As $\sigma_{10}\pi<1$ always, we then take

$$(e^{\sigma_{10}\pi}-1)\approx\sigma_{10}\pi+\frac{(\sigma_{10}\pi)^2}{2} , \tag{12}$$

which allows two of the terms containing $\sigma_{01}\pi$ to cancel out:

$$I_+(\pi)=I_r(0)e^{-\sigma_{10}\pi}\left[1-e^{-\sigma_i\pi}+\frac{\sigma_{01}(\sigma_{10}\pi)^2}{2\sigma_{10}}\right] , \tag{13}$$

where σ_{10} and σ_{01} are cross sections for electron capture by He^+ and electron loss by He, respectively. Using published values for σ_{01} [17,18] and σ_{10} [19–22] along with typical values of π reveals that the third term in the brackets is negligible, yielding the equation

$$\ln\left[1-\frac{I_+}{I_r(0)}e^{\sigma_{10}\pi}\right]=-\sigma_i\pi , \tag{14}$$

to which our data were fit in order to extract σ_i. As a check, notice that this reduces to Eq. (6) as σ_{10} approaches zero. A sample of experimental ionization data fitted to Eq. (14) is shown in Fig. 3.

An additional undesired effect is that of contamination of the signal from the presence of metastable H or He atoms; it is known [23] that the neutralization process used to make the Rydberg atoms will also yield a large fraction of metastable atoms. Metastable H or He can be quenched in an electric field by the field's mixing of the metastable $2s$ state with the short-lived $2p$ state. If the quenching rates of the metastables in the modulator were

different for the high and low fields, the apparatus would produce a spurious modulated signal indistinguishable from Rydberg atoms.

The lifetime of an H($2s$) atom in an electric field F is determined by a parameter $\xi = F/(475\ \text{V/cm})$ [24]. For $\xi \gg 1$, as is the case in the modulator, the lifetimes of both (spin-up and spin-down) $2s$ states are twice that of the $2p$, or 3.2 nsec. This is of the same order as the transit time through the field, so the fraction of metastables quenched is sensitively dependent on the beam speed. Nevertheless, since $\xi \gg 1$ for *both* values (F_{hi} and F_{lo}) of the modulator field, the *difference* in the quenched fraction, and thus the modulated signal, is negligible. There is empirical evidence to support this from a similar experiment in this laboratory [25] using the same apparatus to study collisions of the H metastables; in that experiment, far smaller modulator fields (~ 500 V/cm) were necessary to see a measurable modulated H($2s$) signal.

Helium is, however, somewhat more complicated. Quenching rates for metastable He were calculated by Holt and Krotkov [26]; in an electric field F, the $2\,^1S$ state is mixed with the $2\,^1P$, which can decay to the ground state, to give a decay rate γ of

$$\gamma = (0.89 \pm 0.04) F^2\ \text{sec}^{-1}\ , \tag{15}$$

where F is in kV/cm. Decay of the $2\,^3S$ state would involve a spin flip, so this state cannot be quenched by a laboratory electric field. In Holt and Krotkov's experiment, a 226-kV/cm field quenched 90% of the singlet metastables but left the triplets unaffected.

The fraction of the ion signal coming from He metastables can then be estimated. McCullough, Goffe, and Gilbody [23] measured the fraction of metastables from He^+ electron capture from Na at 2.5 keV/amu to be about 50% and stated that this was a lower limit to the true fraction. Since only the $2\,^1S$ concerns us, we need to know the $2\,^1S/2\,^3S$ ratio. Observations by McCullough, Goffe, and Gilbody indicate that the ratio is very small. To calculate an estimate we assume that *all* capture is to the $n=2$ state and that the magnetic sublevels are populated with equal probability. (For a Cs target, experimental evidence is consistent with this [23], while for our Na target, whose valence level is nearly resonant with He ($2\,^3S$), it is certainly a worst-case estimate.) The $2\,^1S$, $2\,^3S$, $2\,^1P$, and $2\,^3P$ states are then populated in the ratio 1:3:3:9. After radiative decay, the ratio for the $1\,^1S$, $2\,^1S$, and $2\,^3S$ would be 3:1:12, thus leaving $\frac{1}{16}$ or 6% of the beam in the $2\,^1S$ state. Applying Eq. (15) to our experimental conditions gives an estimate of 1.2×10^{-6} of $6\% = 7.5\times10^{-8}$ of the beam that can contribute to the modulated ion signal. Data taken at 2.5 keV/amu show that the Rydberg atoms comprised a 2.5×10^{-5} fraction of the beam, or that the Rydberg fraction is about 300 times bigger than the metastable fraction in this worst-case scenario.

Where cross sections for He($2\,^1S$) much larger than those for He(Rydberg), this small fraction would still represent a problem. However, McCullough, Goffe, and Gilbody also found that the destruction cross sections were about 10 to 15 Å^2 over the (5–100)-keV energy range. A measurement of the destruction cross section for the neutral beam conducted in this lab as a check was consistent with the McCullough results. Thus we conclude that metastables supply much less than 1% of our experimental ion signal and can be neglected.

III. RESULTS

The independent-particle model is illustrated by the data shown in Fig. 4, which shows present measurements of both destruction and ionization cross sections for D ($13 \le n \le 16$) on Xe. Electron-capture cross sections σ_{10} [27], equal-velocity free-electron scattering cross sections σ_e [28], and the sum of the two are shown compared to our data; note that the top scale on the graph is the translational kinetic energy of the equal-velocity quasifree Rydberg electron. Vertical error bars were estimated from the spread in the measured values of the cross sections; the points represent the average of several measurements.

Good agreement with the model is seen; destruction cross sections follow the prediction of Eq. (2) and ionization cross sections follow the prediction of Eq. (1). Data were also taken for H ($13 \le n \le 16$) on N_2 between 10 and 30 keV/amu but are not shown separately; they also verify IPM (H* ionization data are shown in Fig. 7).

The deep Ramsauer-Townsend minimum [29] for electrons scattering from Xe is clearly seen in the figure at about 0.8 eV; it could be sampled by quasifree electrons from projectile Rydberg atoms in the (1–2)-keV/amu range. Apparatus limitations prevented the production of a sufficiently intense H or D beam in that range; hence the switch was made to He projectiles, with which this

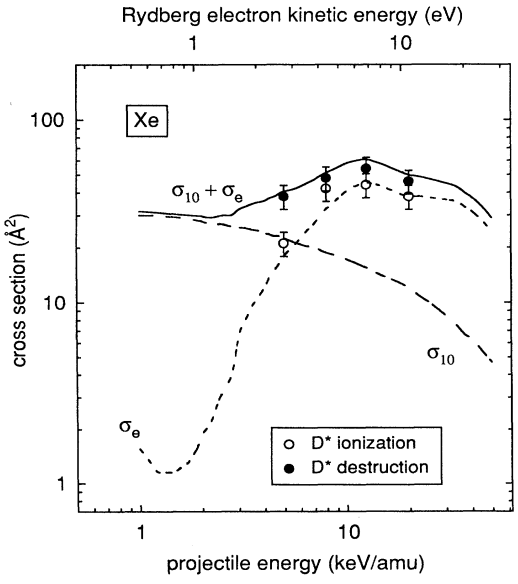

FIG. 4. Independent-particle model. The top energy scale gives the equivalent kinetic energy of the quasifree Rydberg electron attached to a projectile Rydberg atom, which in turn has energy given by the bottom scale. Destruction cross sections for D* are compared to the sum of σ_{10} [27] and σ_e [28]; ionization cross sections are compared to σ_e alone.

(1–2)-keV/amu range could be probed with a (4–8)-keV beam.

Figure 5 shows our measured cross sections for destruction of He ($12 \leq n \leq 15$) on Ar and Xe in comparison with IPM predictions [19,30,20,28]. Results from Silim and Latimer [5] are included for comparison. Good agreement with the prediction of Eq. (2) for Rydberg atom destruction is seen for both targets. Since, however, the destruction cross section is in both cases dominated at low energies by the core scattering channel, it is instructive to look at the quasifree electron-scattering channel separately by measuring the ionization cross section absolutely. This is especially interesting in view of the Ramsauer-Townsend effect's sensitive dependence on the pure s-wave nature of the incoming electron [29].

Figure 6 thus shows our measured cross sections for ionization of He ($12 \leq n \leq 15$) on Ar and both He ($12 \leq n \leq 15$) and H ($13 \leq n \leq 16$) on Xe in comparison with free-electron scattering data for those two targets [30,28], thus testing Eq. (1) alone. The reader will note that He* ionization cross sections have larger vertical error bars at low energy. As the beam energy was reduced, smaller intensities and worsening signal-to-noise ratio, due primarily to the smaller ion signal near the Ramsauer-Townsend minimum, made the ionization measurement less reproducible, increasing the size of the vertical error bars. Note also that the ionization cross sections now have a *horizontal* error bar. This is because at low energies the orbital speed v_e of the electron, while still much smaller than V, adds or subtracts enough to or from it to induce a significant spread in the electron's translational kinetic energy. Following the method used by Koch [2], the maximum and minimum electron kinetic energies are given by

$$E_{\pm} = \tfrac{1}{2} m (V \pm v_e)^2 \; ; \tag{16}$$

the width of the horizontal error bar is then $\Delta E = E_+ - E_-$. A classical model of the atom [31] is then used to estimate the electron orbital velocity; a microcanonical distribution over all possible Kepler orbits gives an average orbital speed

$$v_e = \frac{16}{3\pi^2} v_n \; , \tag{17}$$

where v_n is the Bohr orbital speed and the effect of averaging over possible orientations of the plane of the electron orbit has been included.

The electron-scattering cross section for Ar exhibits a Ramsauer-Townsend minimum just below the lower limit of our energy range. We see that for Ar σ_i, shown in

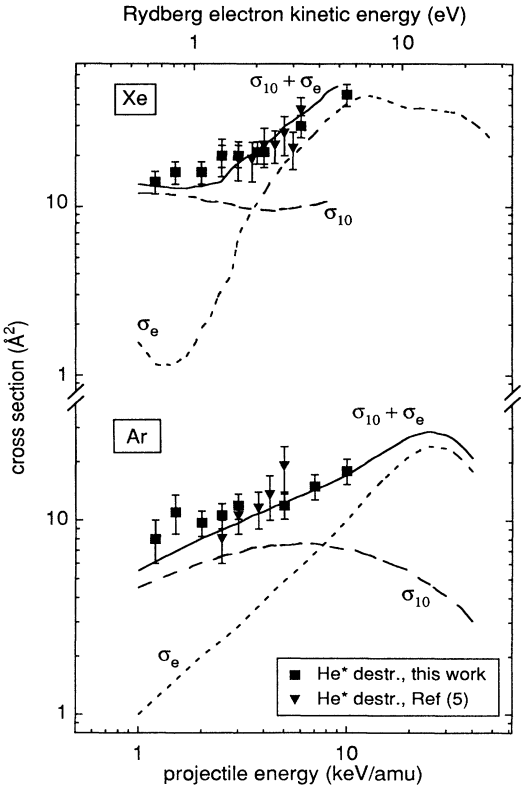

FIG. 5. Destruction cross sections for He* on Xe and Ar targets compared to the sum of σ_{10} and σ_e. Electron-capture data are from Refs. [20] and [19], respectively; electron-scattering data from Refs. [28] and [30]. Good agreement is seen between this work and the data of Ref. [5].

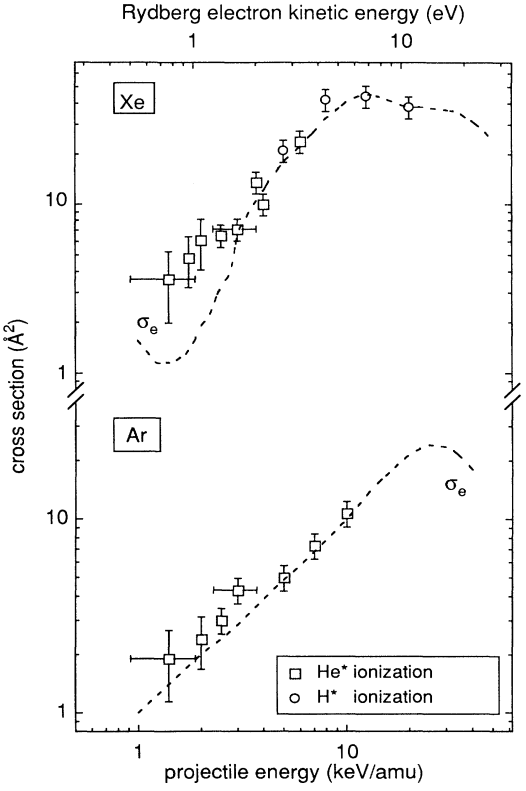

FIG. 6. Ionization cross sections for He* on Xe and Ar, compared to electron-scattering cross sections [28,30]. The departure of Xe data from the quasifree scattering, independent-particle prediction is clearly shown.

Fig. 6, follows the free-electron-scattering cross section as far down as we can measure. In other words, the electron attached to the He core follows the prediction of IPM and scatterers quasifreely.

This is not the case for the Xe target. Pronounced deviation from quasifree scattering behavior is seen below about 3 keV/amu, culminating in a Rydberg ionization cross section at 1.4 keV/amu that is *three times* the predicted value.

This deviation was also seen for He* on a molecular nitrogen target. Figure 7 shows our data for total destruction of He* and for ionization of both He* and H* compared with IPM predictions [32]. Koch's H* ionization data [2] and Silim and Latimer's He* destruction data [5] are included for comparison. While the destruction measurement is in good agreement with IPM, we again see that our ionization measurement is not. Just as in Xe, the Rydberg electron scatters quasifreely at the higher beam energies (whether attached to H^+ or He^+) but fails to do so (when attached to He^+) at the lower energies, starting at about 3 keV/amu. Here the ionization cross section is about twice the IPM prediction at the lowest energy measured. Koch's results do, however, show compliance with IPM for both destruction and ionization of H* on N_2.

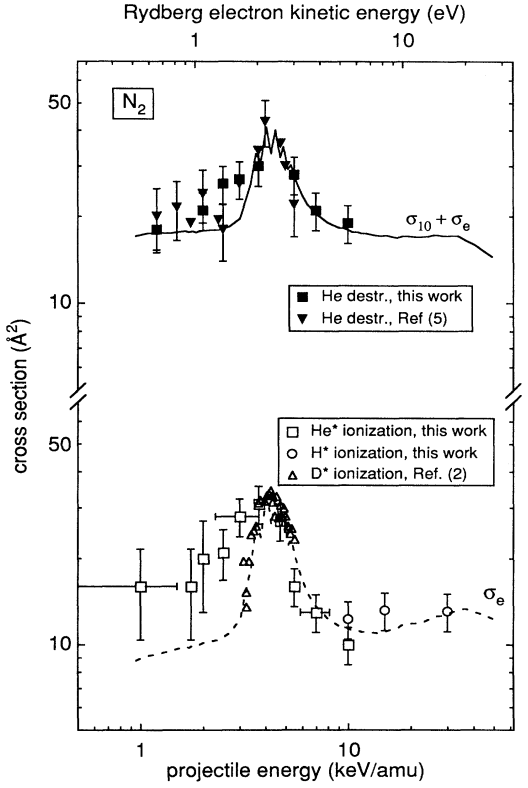

FIG. 7. Destruction cross sections for He* and an ionization cross sections for He* and H* on N_2 compared to the IPM prediction of $\sigma_{10}+\sigma_e$ [13] (for destruction) and σ_e alone (for ionization). The curves has been separated for clarity. Again clear departure from the quasifree scattering prediction for ionization is shown.

It should be noted that at the lower energies frequent checks for systematic error were made by switching target gas from N_2 or Xe to Ar while changing no other experimental parameter. In every case, it was found that Ar would follow IPM and N_2 or Xe would not.

IV. DISCUSSION

Some possible explanations for the Rydberg atoms' behavior in low-energy collisions with Xe and N_2 can be eliminated here. In the first place, one will recall that the quasifree interaction between the Rydberg electron and neutral target is that between a monopole and induced dipole. Xe is considerably more polarizable than Ar; its polarizability is $\alpha=4.1\times10^{-24}$ cm^3 as opposed to 1.64×10^{-24} cm^3 for Ar [33]. One might suspect the stronger and longer-ranged electron-Xe interaction of causing IPM to break down. This cannot, though, explain the N_2 results, as for the nitrogen molecule $\alpha=1.74\times10^{-24}$ cm^3; this is not significantly different from Ar.

Up until now, we have described ionizing collisions, under IPM, as occurring when the Rydberg electron scatters from the target and the Rydberg atom core is a spectator. There are, though, possible means for core scattering to cause ionization of the Rydberg atom. Smirnov [34] has proposed the following collision mechanism. It is possible for the H^+ or He^+ core to scatter *elastically* from the target and leave the collision region at a small angle. This implies that transverse momentum is transferred to the core in the laboratory frame of reference, while *no* momentum is transferred to the Rydberg electron. In the Rydberg atomic core reference frame, this is seen as a momentum change of the electron. By calculating the momentum transfer and comparing it to that necessary to remove the electron from the core, Smirnov calculates a Rydberg atom ionization cross section σ_S:

$$\sigma_S=4.8\left[\frac{\alpha nh}{2\pi MV}\right]^{1/2}\ \text{(cgs units)}\ , \tag{18}$$

where n is the Rydberg atom's principal quantum number, M is the Rydberg ionic core's mass, and V is the beam speed. This scattering mechanism is different from the two mentioned in Eq. (2) in that core scattering ionizes the Rydberg atom. Therefore this cross section must be added to Eq. (1):

$$\sigma_i(E)=\sigma_e\left[\frac{m}{M}E\right]+\sigma_S(\tfrac{1}{2}mV^2)\ . \tag{19}$$

For Xe, σ_S ranges from 0.66 to 0.50 Å^2, while in Ar it is between 0.42 and 0.28 Å^2. This is not enough to bring the Xe data into agreement with IPM, while it leaves the argon target's IPM behavior unaffected. Clearly σ_S will be far too small to affect the nitrogen target's ionization cross sections. Nitrogen, of course, has a permanent quadrupole moment as well. An estimate [35] of the Smirnov-type scattering from the quadrupole potential yields, however, cross sections only on the order of 10^{-3} Å^2, which would be even less significant. This calcula-

tion and application of the Smirnov model cannot, then, explain the results.

There is another core-scattering mechanism that could produce ionization of the Rydberg atom under certain conditions. At low-keV collision energies—where we see IPM breaking down—charge exchange is frequently explained by traversal of and transitions between energy levels in the quasimolecule formed between the collision partners. Charge exchange between partners A^+ and B can take place at close avoided crossings between the levels A-B^+ and A^+-B. If, however, those levels are closely separated as internuclear separation goes to infinity, exchange can occur *more than once* during the outgoing part of the collision process due to coupling between the levels. A classical approximation is to view the exchanged electron as jumping back and forth between A^+ and B^+. It must be remembered, however, that in the presence of parallel molecular levels quantum-mechanical coupling can allow this multiple exchange to take place at large internuclear distances. An even number of electron exchanges in this process will make it appear as if nothing happened during the collision. We will see below that a model consistent with our results in fact *requires* charge exchange to take place at very large internuclear distances.

We suggest that the Rydberg electron may be sensitive to this core-target interaction. Recall that in IPM, if the core captures a target electron, the quasifree Rydberg electron is not only no longer bound but also sees a charged target from which to scatter. This leaves the projectile as a *neutral* atom, usually in the ground state. The multiple-exchange process described above could, however, produce an *ionized* projectile. Were a target electron to be exchanged more than once during the collision, the Rydberg electron would see its binding force repeatedly changed. We imagine this as happening (as mentioned above) as the core leaves the collision region. Were the Rydberg electron properly localized, it could be closer to the target than to the core. Thus, during the time while the binding force was sufficiently reduced, the electron would receive an strong impulse from the now charged target via the Coulomb force—it would see an *enhanced target.* This impulse will impart kinetic energy to the electron. If the kinetic energy added were greater than the Rydberg atom's binding energy, the electron would fail to return to the Rydberg atom even after this binding force became strong enough again. For an even number of target electron exchanges, this would leave a neutral target and an ionized projectile. That is, although the initial and final states of the heavy particle system are identical, the *transient* state formed during the collision forms an enhanced collision target for the Rydberg electron and results in extra ionization not included in IPM. As the Rydberg atom ionization cross section due to this process depends not only on core-target interactions but also on the Rydberg atom's internal interactions, the Rydberg atom's core and electron are no longer independent.

Intermolecular potential curves for the He^+-Ar system [36] and the He^+-Xe system [37] show interesting qualitative differences that may explain our results within the framework outlined above. In the first system, the asymptotic He^+-Ar ground state corresponds to the molecular $B\,^2\Sigma$ state, which experiences several well-isolated curve crossings with other molecular states that tend asymptotically to He-Ar^+; the closest is the $C\,^2\Sigma$ state, which is asymptotically separated from the B state by about 4 eV. The xenon case is, however, quite different, as the initial He^+-Xe level is almost degenerate with several molecular levels tending to He-Xe^+; in particular, the entrance He^+-Xe channel, although 12.5 eV away from the ground charge-exchange exit channel He-Xe^+ ($5p^5\,^2P$), is parallel to and separated by only ~ 0.2 eV from an exit channel leaving the target ion in an excited state, He-Xe^+($6s\,^4P$). This close level could provide the coupling necessary for the enhanced-target scattering mechanism described above, while the He-Ar^+ quasimolecule lacks the necessary levels for this to occur.

That leaves the He* on N_2 measurement, which failed to follow IPM, and the H* on N_2 measurement of Koch [2], which did follow it. Intermolecular potentials for these cases are not available, but we can predict behavior based on the energy levels of the free atoms and molecules involved. Consider the He* case. The energy defect between the incoming He^+-N_2 level and the lowest He-N_2^+ level is given by the difference in the ionization potentials of He and N_2, 24.6 and 15.5 eV, respectively [38]. The incoming channel thus lies 9.1 eV above the lowest He-N_2^+ level. We look, then, for an excited N_2^+ level degenerate with the incident He^+-N_2 level, or 9.1 eV above the ground state. Inspection of the molecular levels for N_2^+ [38] reveals that its $C\,^2\Sigma_u^+$ ($v=5$) level is not only almost exactly 9.1 eV above the ground-state ($v=0$) level but also that the appropriate transition is Franck-Condon favored. Thus it is likely that the mechanism for the failure of IPM in the He* on Xe case and the He* on N_2 case is the same.

The H* on N_2 case is immediately seen to be different, as the H atom ionization potential of 13.6 eV places the outgoing H-N_2^+ channel *above* the incoming H^+-N_2 channel. The ground-state channels, as in all cases mentioned, are too far apart for the close coupling described above to occur, while excited levels of the N_2^+ are even farther away. The enhanced target cannot form, and the Rydberg electron scatters in compliance with IPM.

We can make the following rough quantitative estimate of this effect by estimating the velocity change imparted to the Rydberg electron by the enhanced target (in a manner similar to Smirnov's analysis). Consider the Rydberg electron to be a free electron with speed v passing a fixed charge e with impact parameter b. For small scattering angles the total force applied perpendicular to the electron's initial path is given by

$$F=\frac{8e^2}{3b^2}\ . \tag{20}$$

Assume that the Coulomb force F from the target is repeatedly turned on and off by the putative multiple target electron exchanges. We consider here the force exerted during the electron exchange. If the projectile moves a distance d while the target is ionized, the velocity change

of the (former) Rydberg electron is derived from the impulse applied by F as

$$\Delta v = \frac{8e^2 d}{3b^2 m_e v} . \quad (21)$$

We then assume that the Rydberg atom is ionized if Δv yields enough kinetic energy to overcome the ionization potential W, or if $(\Delta v)^2 \geq 2W/m_e$. This condition combined with Eq. (21) yields a critical impact parameter b_c for ionization; we have

$$b_c^2 = \tfrac{8}{3} d \frac{e^2}{v\sqrt{2Wm_e}} , \quad (22)$$

with the enhanced-target ionization cross section given by

$$\sigma_{ET} = \pi b_c^2 . \quad (23)$$

We now need some reasonable estimate for d, the distance the Rydberg core moves while it has captured the target electron. This is difficult to supply from first principles, as it will depend on the frequency with which the target electron is exchanged between collision partners, which in turn depends on the size of the level coupling. For the He* on N_2 case, the ionization cross section is higher than the IPM prediction by about 10 Å^2 at 3 keV/amu. Our model requires that charge-exchange oscillations take place at large internuclear separation due to close-coupled molecular levels. Let us assume that the coupling is so small that the core moves only $d = 0.5$ Å during the event. For the case of a He ($n = 10$) atom at 3 keV/amu, Eq. (23) does yields $\sigma_{ET} = 10$ Å^2, consistent with the experimental results. This implies that the Rydberg electron is only a few Å from the target while charge-exchange oscillations occur between the target and the distant Rydberg atom core.

In conclusion, this study has demonstrated the failure of the independent-particle model as applied to ionizing collisions of fast Rydberg atoms with neutral targets and has presented a possible explanation for the failure based on an assumed ionization mechanism involving the transient interaction between the target and the Rydberg core.

ACKNOWLEDGMENTS

The authors wish to thank W. Lichten and Yu. Demkov for useful comments about scattering mechanisms and T. Bergeman for calculations and insights regarding field ionization as well as D. Cubaynes for experimental assistance and D. Boule and H. Allen for valuable technical assistance with the experiment's early stages. This research was supported in part by the Alden Trust and by Wesleyan University.

*Present address: Department of Physics, North Carolina State University, Raleigh, NC 27695-8202.
†Present address: Department of Radiation Oncology, S.U.N.Y. at Stony Brook, Stony Brook, NY 11794.
‡Permanent address: Instituto de Fisica, U.N.A.M., AP Postal 139-B, Cuernavaca, Moralos 62191, Mexico.

[1] See, for example, the review articles in *Rydberg States of Atoms and Molecules,* edited by R. F. Stebbings and F. B. Dunning (Cambridge University Press, Cambridge, England, 1983), and references therein.
[2] Peter M. Koch, Phys. Rev. Lett. **43**, 432 (1979); see also Chap. 13 of Ref. [1] by the same author.
[3] L.-J. Wang, M. King, and T. J. Morgan, J. Phys. B **19**, L623 (1986).
[4] A. Cachelin, L.-J. Wang, and T. J. Morgan, *Abstracts of Contributed Papers, Proceedings of the 15th International Conference on the Physics of Electronic and Atomic Collisions, Brighton, 1987,* edited by J. Geddes *et al.* (Queen's University, Belfast, 1987).
[5] H. A. G. Silim and C. J. Latimer, Int. J. Mass Spectrom. Ion Proc. **105**, 75 (1991).
[6] A. Pesnelle, C. Ronge, M. Perdix, and G. Watel, Phys. Rev. A **42**, 273 (1990).
[7] K. B. MacAdam, L. G. Gray, and R. G. Rolfes, Phys. Rev. A **42**, 5269 (1990).
[8] M. Matsuzawa, in Chap. 8 of Ref. [1].
[9] H. Martinez, J. de Urquijo, C. Cisneros, and I. Alvarez, Phys. Lett. **146**, 517 (1990).
[10] R. N. Il'in, V. A. Oparin, E. S. Solov'ev, and N. V. Fedorenko, Zh. Tekh. Fiz. **36**, 1241 (1966) [Sov. Phys. Tech. Phys. **11**, 921 (1967)].
[11] J. D. Jackson and H. Schiff, Phys. Rev. **89**, 359 (1953).
[12] J. R. Oppenheimer, Phys. Rev. **31**, 349 (1928).
[13] D. S. Bailey, J. R. Hiskes, and A. C. Riviere, Nucl. Fusion **5**, 41 (1965).
[14] R. N. Il'in, B. I. Kikiani, V. A. Oparin, E. S. Solov'ev, and N. F. Fedorenko, Zh. Eksp. Teor. Fiz. **47**, 1235 (1964) [Sov. Phys. JETP **20**, 835 (1965)].
[15] This classical estimate is valid for hydrogenic Rydberg atoms such as alkali metals; detailed calculations provided by T. Bergeman (private communication) showed it to be a good estimate for He*. See M. G. Littman, M. M. Kash, and D. Kleppner, Phys. Rev. Lett. **41**, 103 (1978) for an enlightening discussion of the differences between H and hydrogenic Rydberg atoms. See also W. van de Water, D. R. Mariani, and P. M. Koch, Phys. Rev. A **30**, 2399 (1984) for experiments involving field ionization of He*.
[16] B. M. McLaughlin and K. L. Bell, J. Phys. B **22**, 763 (1989).
[17] C. F. Barnett and P. M. Stier, Phys. Rev. **109**, 385 (1958).
[18] Ya. M. Fogel', V. A. Ankudinov, and D. V. Pilipenko, Zh. Eksp. Teor. Fiz. **38**, 26 (1960) [Sov. Phys. JETP **11**, 18 (1960)].
[19] Y. Nakai, A. Kikuchi, T. Shirari, and M. Sataka, Japan Atomic Energy Research Institute, Tech. Report No. 83-143, 1984 (unpublished).
[20] J. B. H. Stedeford and J. B. Hasted, Proc. R. Soc. London. Ser. A **227**, 466 (1955).
[21] B. I. Kikiani *et al.*, Zh. Tekh. Fiz. **48**, 2326 (1978) [Sov. Phys. Tech. Phys. **23**, 1332 (1978)].
[22] C. F. Barnett *et al.*, ORNL Report No. 5206, 1977 (unpublished).

[23] R. W. McCullough, T. V. Goffe, and H. B. Gilbody, J. Phys. B **11**, 2333 (1978).
[24] H. Bethe and E. Salpeter, *Quantum Mechanics of One- and Two-Electron Atoms* (Plenum, New York, 1977).
[25] F. Deng, S. Renwick, and T. J. Morgan (unpublished).
[26] Helen K. Holt and R. Krotkov, Phys. Rev. **144**, 82 (1966).
[27] The line was drawn as the best fit through the data of Ref. [17]; J. F. Williams and D. N. F. Dunbar, Phys. Rev. **149**, 62 (1966); V. V. Afrosimov, Yu. A. Mamaev, M. N. Panov, and N. V. Fedorenko, Zh. Tekh. Fiz. **39**, 159 (1969) [Sov. Phys. Tech. Phys. **14**, 109 (1969)]; T. J. Morgan *et al.*, Phys. Rev. A **14**, 664 (1976).
[28] This line was drawn as the best fit through the data of M. S. Dababneh *et al.*, Phys. Rev. A **22**, 1872 (1980); K. Jost *et al.*, in *Abstracts of Contributed Papers, Proceedings of the 13th International Conference on the Physics of Electronic and Atomic Collisions, Berlin, 1983,* edited by J. Eichler *et al.* (ICPEAC e.V., Berlin, 1983); J. C. Nickel, K. Imre, D. F. Register, and S. Trajmar, J. Phys. B **18**, 125 (1985); and K. P. Subramanian and Vijay Kumar, *ibid.* **20**, 5505 (1987).
[29] C. Ramsauer, Ann. Phys. (Leipzig) **64**, 513 (1921); J. S. Townsend and V. A. Bailey, Philos. Mag. **43**, 593 (1922). See E. W. McDaniel, *Atomic Collisions: Electron and Photon Projectiles* (Wiley, New York, 1989), pp. 182–185, for an overview.
[30] Electron scattering on Ar data from W. E. Kauppila, T. S. Stein, G. Jesion, M. S. Dababneh, and V. Pol, Rev. Sci. Instrum. **48**, 822 (1977).
[31] I. C. Percival and D. Richards, Adv. At. Mol. Phys. **11**, 1 (1975).
[32] Electron capture for He^+ on N_2: Ref. [22]. Free-electron scattering: R. E. Kennerly, Phys. Rev. A **21**, 1876 (1980).
[33] V. Staemmler, Chem. Phys. **17**, 187 (1976).
[34] B. M. Smirnov, *Invited Lectures, Review Papers, and Progress Reports of the 9th International Conference on the Physics of Electronic and Atomic Collisions, Seattle, 1975,* edited by J. S. Risley and R. Geballe (University of Washington Press, Seattle, 1976).
[35] S. P. Renwick, Ph.D. thesis, Wesleyan University, 1991.
[36] F. T. Smith, H. H. Fleischmann, and R. A. Young, Phys. Rev. A **2**, 379 (1970).
[37] F. Howorka *et al.*, Phys. Rev. A **26**, 93 (1982).
[38] A. A. Radzig and B. M. Smirnov, *Reference Data on Atoms, Molecules, and Ions* (Springer-Verlag, Berlin, 1980).